Journal of Applied Mechanics and Technical Physics, Vol. 38, No. 2, 1997

A NUMERICAL STUDY OF A VISCOUS SHOCK LAYER ON A PLATE

T. V. Poplavskaya and V. N. Vetlutskii

UDC 532.526

Justification of the Model of a Full Viscous Shock Layer (FVSL). The hypersonic flow around a flat plate with a sharp leading edge at zero incidence is a classical problem in viscous-fluid mechanics. A flat plate in rarefied gas flow gives rise to a wide range of flow regimes. They vary from the regime in which individual molecular collisions at the leading edge are described by the kinetic theory to the downstream continuum regime of the classical boundary layer. Various models for the rarefied hypersonic flow around a plate with a sharp leading edge are presented in [1–3].

The general model for the flow around a plate using the results of [1–4] is shown in Fig. 1. There is a small region of free-molecular flow immediately at the leading edge of the plate. Next follows a continuum region in which the boundary layer generated by viscous phenomena on the surface and the shock wave (SW) interact and merge to such an extent that it is impossible to draw a distinct boundary between them. This "merged" layer is asymptotically transformed to the region of strong interaction. It is here and further downstream that the parameters behind the SW can be calculated from the generalized Rankine–Hugoniot relations. In the strong-interaction region, the inviscid-flow zone between the SW and the boundary layer cannot be clearly distinguished, or this region is small. Further downstream on the plate, a weak-interaction region forms in which inviscid flow plays a substantial role.

Experimental investigations [5–7] deal mainly with the merged layer, which is the intermediate region between the classical hypersonic boundary layer located downstream and the kinetic model of the flow at the leading edge. McCroskey et al. [4] found that the strong-interaction model has a certain upstream limit of applicability where the boundary layer and the shock wave merge. This is the case for $V = \mathrm{M}_\infty\sqrt{C}/\mathrm{Re}_x \simeq 0.1$–$0.2$, where V is a rarefaction parameter that is most suitable for determining the upstream boundary of the strong-interaction region and the computation domain of the viscous shock layer, and C is the Chapman–Rubezin constant).

In the present paper, we consider hypersonic flow around a plate with a sharp leading edge within the framework of the model of a viscous shock layer for values of the rarefaction parameter V of from 0.1 to 0.15, for which the boundary layer merges with the SW, to lower values of V for which the boundary layer is separated from the SW by an inviscid flow region ($V < 0.1$). The FVSL equations describe the entire flow region between the body and the SW. They include all terms of Euler equations and of boundary-layer equations. The advantages of the viscous shock-layer model include

— the calculation of flows with moderately low Reynolds numbers and of flows under conditions of shock-wave–boundary-layer interaction, which is impossible in the classical boundary-layer theory;
— the possibility of avoiding the search for external data for the boundary layer;
— unified calculation of the entire flow field in the regions of both strong and weak interaction;
— the use of a marching approach to solve the FVSL equations;
— economy in comparison with the Navier–Stokes model.

The viscous shock-layer model has been widely used recently for aerohydrodynamic and reentry problems. In most papers [8–12], smooth blunted bodies have been considered. We are unaware of any publications on hypersonic flow around slender bodies with a sharp leading edge within the framework of the viscous shock layer model. Hayes and Probstein [13] obtained approximate analytical solutions of

Institute of Theoretical and Applied Mechanics, Siberian Division, Russian Academy of Sciences, Novosibirsk 630090. Translated from Prikladnaya Mekhanika i Tekhnicheskaya Fizika, Vol. 38, No. 2, pp. 91–100, March–April, 1997. Original article submitted June 29, 1995; revision submitted November 21, 1995.

 0021-8944/97/3802-0250 $18.00

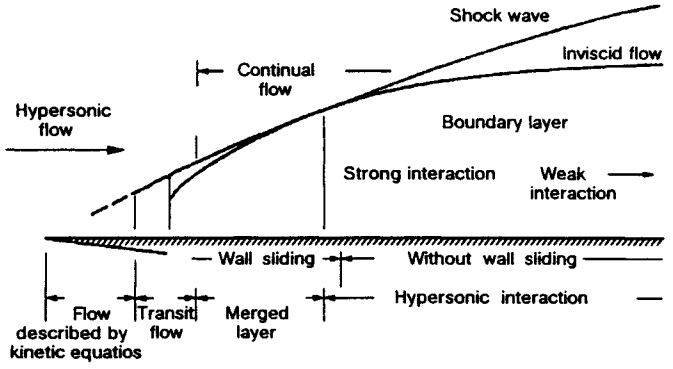

Fig. 1

the hypersonic-boundary-layer equations for the regions of strong and weak interaction separately. Pan and Probstein [14] derived correlation formulas for the pressure and heat transfer on the body surface for air in the merged layer and in the strong-interaction region. Shorenstein and R. F. Probstein [15] derived empirical functions approximating the calculation results for the shock position and density on the shock-wave surface in a local-similar approximation in the merged layer.

Rudman and Rubin [16], using the system of equations describing the boundary layer, the SW structure, and the inviscid core of the flow, considered the hypersonic viscous interaction on slender bodies with a sharp leading edge. Although the focus was on the study of the continuum region (merged layer) at the leading edge, where the rarefaction parameter is $V \sim 1$, Rudman and Rubin believe that the suggested theory is also applicable for lower values of V that correspond to the beginning of the strong-interaction region.

In the present paper, all characteristics (velocity, pressure, density, temperature, and skin-friction and heat-transfer coefficients) of the flow around a plate at zero incidence are calculated within the framework of the viscous shock-layer model over wide ranges of Mach and Reynolds numbers, and the influence of the latter on the flow parameters is studied.

Formulation of the Problem. Let us consider hypersonic flow around a plate with a sharp leading edge at zero incidence. We write the FVSL equations in the Cartesian coordinate system (x, y) in which the x coordinate is directed along the plate surface and y is normal to it. By analogy with [8], these equations can be obtained in the form

$$\frac{\partial \rho u}{\partial x} + \frac{\partial \rho v}{\partial y} = 0, \qquad \rho u \frac{\partial u}{\partial x} + \rho v \frac{\partial u}{\partial y} - \frac{1}{\mathrm{Re}_L} \frac{\partial}{\partial y}\left(\mu \frac{\partial u}{\partial y}\right) + \frac{\partial P}{\partial x} = 0,$$

$$\rho u \frac{\partial v}{\partial x} + \rho v \frac{\partial v}{\partial y} - \frac{4}{3} \frac{1}{\mathrm{Re}_L} \frac{\partial}{\partial y}\left(\mu \frac{\partial v}{\partial y}\right) + \frac{\partial P}{\partial y} = 0,$$

$$c_p \rho u \frac{\partial T}{\partial x} + c_p \rho v \frac{\partial T}{\partial y} - \frac{1}{\mathrm{Pr}} \frac{1}{\mathrm{Re}_L} \frac{\partial}{\partial y}\left(k \frac{\partial T}{\partial y}\right) - \frac{1}{\mathrm{Re}_L} (\gamma - 1) \mathrm{M}_\infty^2 \mu \left(\frac{\partial u}{\partial y}\right)^2 - \tag{1}$$

$$-\left(\gamma - 1\right) \mathrm{M}_\infty^2 \left(u \frac{\partial P}{\partial x} + v \frac{\partial P}{\partial y}\right) = 0, \qquad P = \frac{1}{\gamma \mathrm{M}_\infty^2} \rho T,$$

where u and v are the velocity components in the x and y directions, P is the pressure, T is the temperature, $\mathrm{Pr} = \mu_\infty c_{p\infty}/k_\infty$ is the Prandtl number, and $\mathrm{Re}_L = \rho_\infty U_\infty L/\mu_\infty$ is the Reynolds number determined from the free-stream parameters and the model length L. The velocity components are made dimensionless with respect to the free-stream velocity U_∞, the pressure is referred to the doubled velocity head $\rho_\infty U_\infty^2$, the viscosity μ, the heat conductivity k, the specific heat c_p, the density and temperature are normalized to their free-stream values, and the x and y coordinates are referred to the model length L. Exactly these variables are presented in the graphs unless otherwise specified.

The FVSL equations describe the entire flow region between the plate and the SW. In addition to all terms of boundary-layer equations, they include a conservation equation for momentum projected onto the normal to the plate. All terms of the Euler equations are also retained here.

We consider Mach and Reynolds numbers for which a thin SW forms, since only in this case can the generalized Rankine–Hugoniot relations be used as boundary conditions for the SW [17]:

$$u_s = \cos^2\beta(1 + k_s\tan^2\beta) - \frac{\mu_s(1-\tan^2\beta)\cos^3\beta}{\mathrm{Re}_L\sin\beta}\frac{\partial u}{\partial y}, \qquad v_s = u_s\tan\beta - k_s\tan\beta,$$

$$P_s = \frac{1}{\gamma \mathrm{M}_\infty^2} + (1-k_s)\sin^2\beta - \frac{2\mu_s\sin\beta\cos\beta}{\mathrm{Re}_L}\frac{\partial u}{\partial y}, \tag{2}$$

$$H_s = 1 + \frac{\gamma-1}{2}\mathrm{M}_\infty^2 - \frac{\cos\beta}{\sigma_s \mathrm{Re}_L\sin\beta}\left[\frac{\partial H}{\partial y} - \frac{1-\mathrm{Pr}}{2}(\gamma-1)\,\mathrm{M}_\infty^2\frac{\partial u^2}{\partial y}\right], \quad k_s = \frac{1}{\rho_s}, \quad \gamma = \frac{c_{p\infty}}{c_{v\infty}}, \quad \sigma_s = \frac{\mathrm{Pr}}{\mu_s}.$$

Here H is the total enthalpy, β is the SW angle, γ is the adiabatic exponent for the free stream, and the subscript s indicates the flow parameters behind the SW. The integral condition of equal mass flow on both sides of the shock wave is used to determine the SW shape $y_s(x)$.

The slip and temperature-jump conditions are used as boundary conditions for the plate [18]:

$$u_w = 1.252\frac{(2-\alpha_u)\mu}{\alpha_u \mathrm{Re}_L\sqrt{P\rho}}\left.\frac{\partial u}{\partial y}\right|_w, \quad T = T_w + 2.5\frac{(2-\alpha_T)\gamma\mu}{\alpha_T(\gamma+1)\mathrm{Re}_L\,\mathrm{Pr}\sqrt{P\rho}}\left.\frac{\partial T}{\partial y}\right|_w. \tag{3}$$

Here α_u is the slip coefficient and α_T is the accommodation coefficient.

For a convenient calculation of system (1), we introduce a new independent variable $\bar{y}$ along the normal, so that the difference grid has a constant number of steps between the body and the SW. Furthermore, new dependent variables are introduced by normalizing all parameters to their local values behind the SW: $\bar{x} = x$, $\bar{y} = y/y_s(x)$, $\bar{u} = u/u_s$, $\bar{v} = v/v_s$, $\bar{T} = T/T_s$, $\bar{P} = P/P_s$, $\bar{\rho} = \rho/\rho_s$, and $\bar{\mu} = \mu/\mu_s$. Then, the momentum and energy equations in the transformed variables $\bar{x}$ and $\bar{y}$ can be written in the standard form for parabolic equations (the bars are omitted):

$$a_i\frac{\partial f_i}{\partial x} + b_i\frac{\partial f_i}{\partial y} + \frac{\partial}{\partial y}\left(c_i\frac{\partial f_i}{\partial y}\right) + d_i = 0, \tag{4}$$

$$f_1 = u\text{: } a_1 = \rho_s u_s^2\rho u,\ b_1 = (\rho_s u_s/y_s)\rho(-yu_s u\tan\beta + v_s v),\ c_1 = -\frac{1}{\mathrm{Re}_L}\frac{1}{y_s^2}\mu_s u_s\mu,\ d_1 = P_s\frac{\partial P}{\partial x} - yP_s\frac{\tan\beta}{y_s}\frac{\partial P}{\partial y},$$

$$f_2 = v\text{: } a_2 = \rho_s u_s v_s\rho u,\ b_2 = (\rho_s v_s/y_s)\rho(-yu_s u\tan\beta + v_s v),\ c_2 = -\frac{4}{3}\frac{1}{\mathrm{Re}_L}\frac{1}{y_s^2}\mu_s v_s\mu,\ d_2 = \frac{P_s}{y_s}\frac{\partial P}{\partial y},$$

$$f_3 = T\text{: } a_3 = c_p\rho_s u_s T_s\rho u, \quad b_3 = \frac{c_p\rho_s T_s}{y_s}\rho(-yu_s u\tan\beta + v_s v), \quad c_3 = -\frac{1}{\mathrm{Pr}}\frac{1}{\mathrm{Re}_L}\frac{1}{y_s^2}\mu_s T_s k,$$

$$d_3 = -\frac{1}{\mathrm{Re}_L(\gamma-1)\mathrm{M}_\infty^2}\frac{\mu_s u_s^2}{y_s^2}\mu\left(\frac{\partial u}{\partial y}\right)^2 - (\gamma-1)\mathrm{M}_\infty^2\left[u_s P_s u\frac{\partial P}{\partial x} + \frac{P_s}{y_s}\frac{\partial P}{\partial y}(-yu_s u\tan\beta + v_s v)\right].$$

The continuity equation takes the form

$$\rho_s u_s\frac{\partial\rho u}{\partial x} + \frac{\rho_s}{y_s}\left(-yu_s\tan\beta\frac{\partial\rho u}{\partial y} + v_s\frac{\partial\rho v}{\partial y}\right) = 0; \tag{5}$$

the equation of state is

$$P = (1/(\gamma\mathrm{M}_\infty^2))\,(\rho_s T_s/P_s)\rho T. \tag{6}$$

The parameters behind the SW now enter into the basic equations (4)–(6) as unknown coefficients, and the boundary conditions for the SW become $u = v = T = \rho = 1$ for $y = 1$. In the computations, viscosity was approximated by Sutherland's law.

Initial Conditions. Analysis of the experimental data of [1, 4–6] showed that at the sharp edge, at the end of the merged layer, and at the beginning of the region of strong shock-wave–boundary-layer interaction, viscous flow occupies the entire region between the plate surface and the undisturbed flow, and there is no distinct inviscid flow in this region. Therefore, we describe the entire disturbed region by boundary-layer

equations, by replacing the SW by a discontinuity surface, although the SW thickness in this region is on the same order as the boundary-layer thickness. The latter assumption can introduce a certain error in a solution that is used as the initial condition for $x = x_0$. However, because of the parabolicity of the FVSL equations, this error rapidly decays downstream. For $x = x_0$, the system of FVSL equations (1) can be reduced to ordinary differential equations using the transformation $\xi = x$ and $\eta = y\sqrt{\mathrm{Re}_L}/\sqrt{x}$, which is typical of boundary-layer flows with a uniform external flow. In the variables ξ and η, the system of equations for the initial cross section $x = x_0$ takes the form

$$\frac{dJ}{d\eta} + \frac{1}{2}\rho u = 0, \quad J = \sqrt{\xi}\rho v - 0.5\rho u\eta, \quad J\frac{du}{d\eta} - \frac{d}{d\eta}\left(\mu\frac{du}{d\eta}\right) = 0, \quad \frac{dP}{d\eta} = 0,$$
$$c_p J\frac{dT}{d\eta} - \frac{1}{\mathrm{Pr}}\frac{d}{d\eta}\left(k\frac{dT}{d\eta}\right) - (\gamma-1)\mathrm{M}_\infty^2\mu\left(\frac{du}{d\eta}\right)^2 = 0, \quad P = \frac{1}{\gamma\mathrm{M}_\infty^2}\rho T. \tag{7}$$

We solve system (7) subject to the boundary conditions

$$\eta = 0: \quad J = 0, \quad u, T \quad \text{are calculated from} \quad (3),$$
$$\eta = \eta_s: \quad u = u_s, \quad v = v_s, \quad T = T_s, \quad \rho = \rho_s.$$

Here η_s (the SW detachment) is found from the mass balance relation for the shock layer under the assumption of a straight SW in the interval $0 \leqslant x \leqslant x_0$.

Difference Scheme and Algorithm of Solution. The nonlinearity of system (4)–(6) requires an iterative approach which reduces the problem within one iteration to a sequential solution by the sweep method of the difference boundary-value problems approximating equations (4)–(6): $A_nW_{n+1} + B_nW_n + C_nW_{n-1} + D_n = 0$. Here n is the difference-grid node number with respect to the y coordinate. The boundary conditions on the body are obtained by writing the slip and temperature-jump conditions (3) in terms of one-side differences for three points. Moreover, for the body surface, we add the condition $\partial P/\partial y = 0$, from which we obtain an additional condition for density using the equation of state (6). The SW conditions now reduce to the equality $W = 1$ for all parameters.

The algorithm of solution of the FVSL equation is as follows. We first solve the ordinary differential equations (7) near the leading edge. The Mach cone angle is used as the initial value of the slope β in finding the SW position. The thus-obtained profiles u_0, v_0, T_0, P_0, and ρ_0 are set as the initial conditions in the cross section $x = x_0$.

Then, the viscous shock-layer equations are solved by the marching method with respect to the x-coordinate. We first determine the velocity components and temperature from the equations of motion and energy. Next, the density is determined from the continuity equation, and finally, the pressure is found from the equation of state. Generally speaking, this problem is not correct, since system (4)–(6) is not rigorously parabolic, and disturbances can be transported upstream along the subsonic part of the boundary layer. Some regularization is needed to suppress these disturbances. The method used in the present work is based on the idea of sublayer approximation [19], according to which the term $\partial P/\partial x$ is calculated outside the subsonic region and is introduced in this region as a constant quantity.

For the values of u, v, T, P, and ρ obtained for the given value of x, the condition of the mass-flow conservation with passage through the SW is verified. If this condition is not satisfied for the given values, the SW angle β is corrected by a small quantity ε. The SW parameters are calculated from the new value of β, and the above algorithm of solution for system (4)–(6) is used again.

The solution of the problem yields the velocity, temperature, density, and pressure profiles over the entire shock layer. They are used to calculate the skin-friction coefficient on the plate surface,

$$C_f = \mu\frac{\partial u}{\partial y}\Big|_{y=0} \Big/ 0.5\rho_\infty U_\infty^2,$$

and the heat-transfer coefficient St (the Stanton number). The latter takes into account the "sliding-friction"

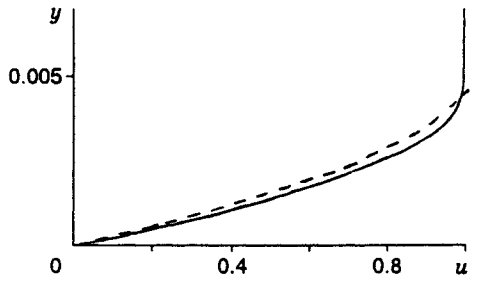

Fig. 2

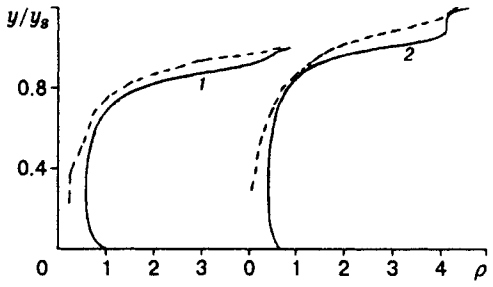

Fig. 3

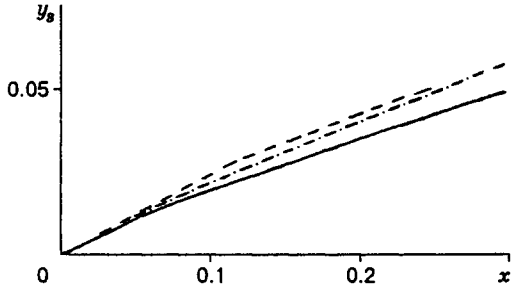

Fig. 4

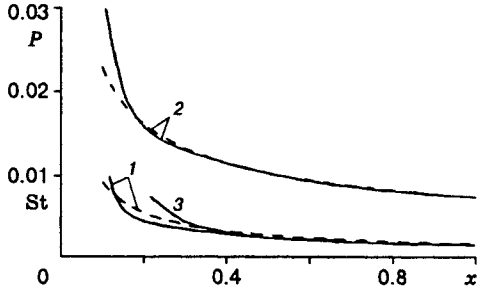

Fig. 5

energy transfer under the slip boundary conditions, as in [16]:

$$\mathrm{St} = \left(k\frac{\partial T}{\partial y} + u\mu\frac{\partial u}{\partial y}\right)\Big|_{y=0} \Big/ \rho_\infty U_\infty (H_\infty - H_w).$$

Computation Results. Several test computations were carried out to validate the algorithm and the results obtained.

The dashed curve in Fig. 2 shows the velocity values obtained analytically by Hantzsche and Wendt and borrowed from [18] for a laminar boundary layer on a plate positioned streamwise in a supersonic flow ($M_\infty = 5$, $Re_L = 5 \cdot 10^5$, $Pr = 0.7$, and $T_w = T_\infty$). The solid curve in this figure represents the velocities obtained in the present work using the algorithm of solution for the FVSL equations in the cross section $x = 0.17$. Evidently the difference is less than 7%. In the given variant of computation ($M_\infty = 5$), the boundary layer amounts to only 1/8 of the shock layer, and comparison of u profiles is presented for this region, i.e., up to $y \approx 0.005$.

The flow field on a flat plate in the merged-layer regime is experimentally studied by McCroskey et al. [4]. The results are obtained based on a combination of several probing and optical methods and surface-pressure measurements. The density was calculated using combined measurements, and its accuracy, as is noted in [4], is within $\pm 10\%$ in the strong-interaction region and within $\pm 20\%$ upstream in the merged layer.

Figure 3 shows density profiles in the cross sections $x = 0.14$ and 0.21 (curves 1 and 2). For $M_\infty = 24.5$, $Re_1 = 3.94 \cdot 10^5$ m^{-1}, $T_0 = 2000$ K, and $T_w = 295$ K, the cross section $x = 0.21$ corresponds to the strong-interaction region and the cross section $x = 0.14$ to the merged layer. The solid curve shows the density profiles calculated from the FVSL equations as functions of the dimensionless coordinate y normalized to its value at the SW, and the dashed curve represents the results of [4]. The disagreement between the results can be explained by the fact that, on the one hand, both cross sections are located in the region of transition from the merged-flow regime to the strong-interaction regime, i.e., in the region of flow restructuring, and on the other hand, neither of the above-mentioned experimental techniques is a direct method.

Figure 4 shows a comparison of the SW detachment distance at $M_\infty = 24.5$, $Re_1 = 5.9 \cdot 10^5$ m^{-1}, $T_0 = 2000$ K, and $T_w = 300$ K with the data of [4]. The dot-and-dashed curve indicates the SW position

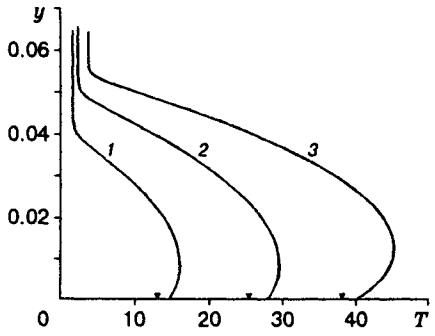

Fig. 6

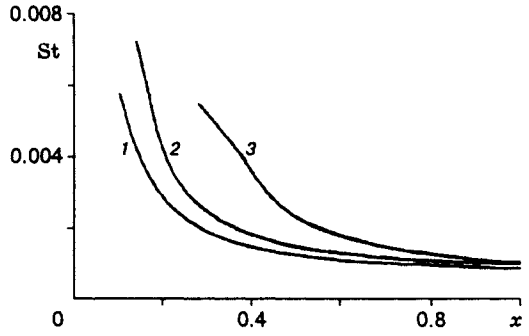

Fig. 7

calculated from the formula of [15], and the remaining notation is the same as in Fig. 3. The disagreement is within the experiment accuracy.

Pan and R. F. Probstein [14] present approximation formulas for the pressure and heat-transfer distributions on the surface which correspond to the solution in the strong-interaction region (subscript SI):

$$P_{SI} = (0.554T_w/T_0 + 0.0973)\mathrm{M}_\infty^3\sqrt{C/\mathrm{Re}_x},$$
$$\mathrm{St}_{SI} = (0.368T_w/T_0 + 0.0684)\left[\mathrm{M}_\infty\sqrt{C/\mathrm{Re}_x}\right]^{3/2}. \tag{8}$$

Here C is the Chapman–Rubezin constant for a linear dependence of viscosity on temperature [20]. It is important that the constant C in formulas (8) makes a substantial contribution to the P and St distributions. However, the value of this constant varies greatly (~15–20%), depending on how it is calculated: in terms of the reference temperature following Cheng's definition [20] or using values of μ_∞ and T_∞ [14].

Figure 5 shows a comparison of the values of St_{SI} and P_{SI} (dashed curves 1 and 2, respectively) with those calculated in the present paper (solid curves 1 and 2) for the same flow conditions as in Fig. 3. The Chapman–Rubezin constant is 0.72, as in [4]. A small difference in pressure along the surface is observed only near the boundary of the merged layer at $x = 0.135$, which corresponds to the rarefaction parameter $V = 0.15$. Solid and dashed curves 1 merge in the region of strong interaction which is extended up to the plate end (the parameter $\chi_\infty = \sqrt{C}\mathrm{M}_\infty^3/\sqrt{\mathrm{Re}_x} \gg 4$ everywhere). The difference in heat fluxes is within 10% on the main part of the plate and within 18% near the merged layer edge. It should be noted that the marching method implies that there is a zone of influence of the initial solution of the problem.

Figure 5 shows the calculated Stanton number (curve 3) for the same condition but beginning from the cross section $x_0 = 0.2$, in contrast to the available computations, in which $x_0 = 0.1$ (solid curve 1). Curves 1 and 3 are practically coincident beginning with $x = 0.4$. This means that the influence zone of initial data is about 0.2. It should be noted that the value of St here, as was predicted by the strong-interaction theory, is practically inversely proportional to $x^{3/4}$ rather than to $\sqrt{x}$, as in the classical boundary-layer theory.

Metcalf et al. showed [7] that the SW strength (i.e., $\rho_{\max}/\rho_\infty$) depends only on the parameter $\mathrm{M}_\infty C/\mathrm{Re}_x \sim \mathrm{Kn}_x$ (Kn_x is the Knudsen number), at least at a distance of 100 mean free paths from the leading edge of the plate. A universal curve of the SW strength versus Kn_x for Knudsen numbers of from 0.001 to 0.2 was plotted using the experimental data of [5–7]. The region of applicability of the FVSL model does not allow computations for $\mathrm{Kn}_x > 0.0015$, but within $\mathrm{Kn}_x \simeq 0.001$–$0.0015$, the difference between the $\rho_{\max}/\rho_\infty$ values in the present work and in the universal curve is less than 3% for $\mathrm{Re}_x \sim 2 \cdot 10^4$–$2 \cdot 10^5$ and $\mathrm{M}_\infty > 20$.

Another validation of the suggested algorithm of solution for the FVSL equations is the good agreement between the calculated density profiles and those measured by the electron-beam fluorescence technique [21].

The advantages of the theoretical approach over the experimental methods include not only the possibility of obtaining a complete picture, i.e., all flow parameters, but also the possibility of conducting

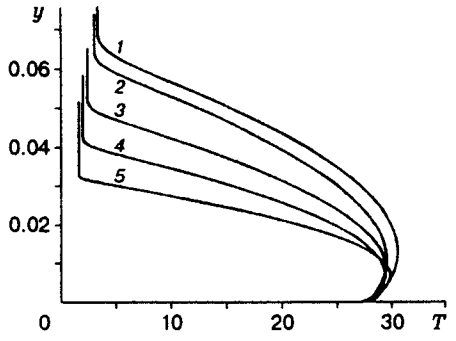

Fig. 8

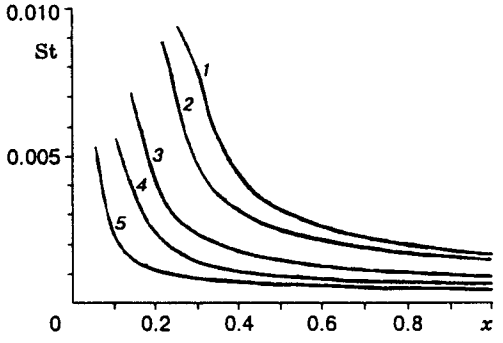

Fig. 9

rapid and easy parametric studies by varying the governing parameters. Basic computations were performed by a scheme that was in good agreement with the experiment of [21] for $M_\infty = 21$, $Re_L = 2.1 \cdot 10^5$, $L = 0.36$ m, $T_0 = 1100$ K, $T_w = 310$ K, $x_0 = 0.1$, Pr = 0.7, and $\alpha_u = \alpha_T = 0.8$. The computations were carried out on a grid with 160 points along the normal and 900 points in the longitudinal direction ($\Delta x = 0.001$). This computation scheme took 20 min of computer time on an IBM PC/AT 486. A twofold increase in the number of grid points in both directions changed the solution by less than 1.5%.

The slip flow changes markedly the velocity and temperature profiles at the plate surface. Therefore, the question arises of when the slip and temperature-jump boundary conditions should be used. Rudman and Rubin [16], using calculations of the merged layer near the leading edge of a plate, showed that it is necessary to use the slip boundary conditions for $\chi_\infty/M_\infty^2 = \sqrt{C}M_\infty/\sqrt{Re_x} > 0.1$ At high Mach numbers, these values are observed in the merged layer and in the region of transition to the strong-interaction regime, i.e., in regions in which the FVSL calculations begin. Thus, the slip and temperature-jump boundary conditions were used in the present paper for all variants. Tsien [22] presents tables of the slip coefficients α_u and the accommodation coefficients α_T for air. They show that for metals, $\alpha_u = 0.79$–1.0 and $\alpha_T = 0.80$–0.97. The slip and accommodation coefficients for the basic variant are within these limits [22] and are chosen from the condition of the best agreement with the experiment of [21].

Figure 6 shows profiles of the dimensionless temperature along the normal for $M_\infty = 15$, 21, and 25 (curves 1–3) in the cross section $x = 0.4$ (all remaining parameters are the same as in the basic variant). The triangles on the abscissa indicate the T_w values. One can see that in the major portion of the viscous layer, the temperature in the viscous region is considerably higher than that in the inviscid region, because of the transformation of dissipation effects. The portion of inviscid flow behind the SW decreases with an increase in M_∞: it is about 1/3 of the shock layer for $M_\infty = 15$ and only 1/6 for $M_\infty = 25$. Computations within the framework of the FVSL model can be carried out for both higher and lower Mach numbers. It should be noted, however, that for $M_\infty < 15$, the inviscid portion is 3/4 of the shock layer (see Fig. 1).

In supersonic flow, the inviscid-flow region decreases with an increase in M_∞, and the SW approaches the body surface. At hypersonic speeds, the boundary-layer thickness is significant, and its increase with an increase in M_∞ can compensate for the decrease in the inviscid region. Therefore, the SW-detachment distance was practically the same for the Mach numbers examined. Figure 7 shows the Mach-number effect on the heat-transfer coefficients (notation is the same as in Fig. 6). As might be expected, the St values increase monotonically over the entire plate length with an increase in M_∞.

The Reynolds-number effect on various flow characteristics are shown in Figs. 8–10. Curves 1–5 correspond to $Re_L = 8 \cdot 10^4$, $1 \cdot 10^5$, $2.1 \cdot 10^5$, $4 \cdot 10^5$, and $8 \cdot 10^5$, respectively. Figure 8 shows normal temperature distributions for various Re_L in the cross section $x = 0.4$. The distance to the SW decreases with an increase in Re_L, and the temperature profiles T are "pressed" to the plate. The Reynolds-number effect is significant over the entire shock layer, in contrast to the Mach number, whose variation exerts a more appreciable effect on the temperature distribution near the plate surface (see Fig. 6). The St values (Fig. 9) decrease monotonically in all cross sections with an increase in Re_L.

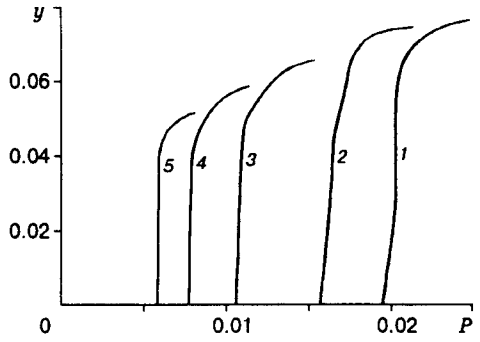

Fig. 10

Figure 10 shows the normal-pressure distributions for various Re_L in the cross section $x = 0.4$. Evidently, the pressure along the normal varies within 20% mainly in the inviscid region behind the SW. For small Re_L, these changes in the boundary layer reach 4%.

The parametric studies showed that the FVSL model adequately describes hypersonic flow around a plate for both high ($\mathrm{Re}_x \sim 10^6$) and moderate Reynolds numbers ($\mathrm{Re}_x \sim 10^4$, Re_x is the local Reynolds number). The computations can also be carried out for lower Re_L but in a smaller domain in the x direction. since the initial cross section should be located at the boundary between the merged layer and the strong-interaction region, and this boundary moves downstream from the leading edge with a decrease in the Reynolds number.

The authors are grateful to Prof. A. A. Maslov for valuable comments.

This work was supported by the Russian Foundation for Fundamental Research (Grant 96-01-01640).

REFERENCES

1. H. T. Nagamatsu, R. E. Sheer (Jr.), and J. R. Schmid, "Flow around the flat plate by the hypersonic flow of rarefied gas at high temperatures," *ARS J.*, **31**, No. 7 (1961).
2. H. Oguchi, "Leading edge slip effects in rarefied hypersonic flow," in: *Rarefied Gas Dynamics*. J. A. Laurmann (ed.), **2** (1963), p. 181.
3. J. A. Laurmann, "Structure of the boundary layer at the leading edge of a flat plate in hypersonic slip flow," *AIAA J.*, No. 2, 1655–1657 (1964).
4. W. J. McCroskey, S. M. Bogdonoff, and J. G. McDougall, "An experimental model for the sharp flat plate in rarefied hypersonic flow," *AIAA J.*, **4**, No. 9 (1966).
5. W. J. McCroskey and J. G. McDougall, "Shock wave shapes on a sharp flat plate in rarefied hypersonic flow," *AIAA J.*, **4**, No. 1 (1966).
6. P. L. Harbour and J. N. Lewis, "Preliminary measurements of the hypersonic rarefied flow on a sharp flat plate using an electron beam probe," in: *Rarefied Gas Dynamics*, C. L. Brundin (ed.) **2**, (1967). pp. 1031–1046.
7. S. C. Metcalf, D. C. Lillicrap, and C. J. Berry, "A study of the effect of surface temperature on the shock-layer development over sharp-edged shapes in low-Reynolds-number high-speed flow," in: *Rarefied Gas Dynamics*, L. Trilling and H. Y. Wachman (eds.), **1** (1969), pp. 619–634.
8. R. T. Davis, "Numerical solution of the hypersonic viscous shock-layer equations," *AIAA J.*, **8**, No. 5. 843–851 (1970).
9. Yu. P. Golovachev and F. D. Popov, "Supersonic viscous flow around a cooled spherical bluntness," *Prikl. Mekh. Tekh. Fiz.*, No. 5, 135–142 (1972).
10. V. G. Voronkin, "Computation of the viscous shock layer at blunted cones," *Izv. Akad. Nauk SSSR. Ser. Mekh. Zhidk. Gaza*, No. 6, 99–105 (1974).

11. I. V. Vershinin, G. A. Tirskii, and S. V. Utyuzhnikov, "Supersonic laminar flow around the windward side of infinite-span swept wings over a wide range of Reynolds numbers," *Izv. Akad. Nauk SSSR, Ser. Mekh. Zhidk. Gaza*, No. 4, 40–44 (1991).
12. S. A. Vasil'evskii, G. A. Tirskii, and S. V. Utyuzhnikov, "A numerical method for solving viscous shock-layer equations," *Zh. Vychis. Mat. Mat. Fiz.*, **27**, No. 5, 741–750 (1987).
13. W. D. Hayes and R. F. Probstein, *Hypersonic Flow Theory*, Academic Press, New York (1959).
14. Y. S. Pan and R. F. Probstein, "Rarefied-flow transition at a leading edge," in: J. Gordon Hall, *Fundamental Phenomena in Hypersonic Flow*, Cornell Univ. Press, New York (1966), pp. 259–306.
15. M. L. Shorenstein and R. F. Probstein, "The hypersonic leading-edge problem," *AIAA J.*, **6**, No. 10, 1898–1906 (1968).
16. S. Rudman and S. G. Rubin, "Hypersonic viscous flow over slender bodies with sharp leading edges," *AIAA J.*, **6**, No. 10, 1883–1890 (1968).
17. G. A. Tirskii, "On the theory of the hypersonic flow of a viscous chemically reactive gas over two-dimensional and axisymmetric blunted bodies with injection," in: *Scientific Papers of Moscow State University Institute of Mechanics*, No. 39, 5–38 (1975).
18. L. G. Loitsyanskii, *Fluid Mechanics* [in Russian], Nauka, Moscow (1973).
19. T. C. Lin and S. G. Rubin, "Viscous flow over a cone at moderate incidence," *J. Comput. Fluids*, **1**, 37–57 (1973).
20. H. K. Cheng, J. H. Gordon, T. C. Golian, and A. Hertzberg, "Boundary-layer displacement and leading-edge bluntness effects in high-temperature hypersonic flow," *J. Aerospace Sci.*, **28**, No. 5, 353–381 (1961).
21. V. N. Vetlutskii, A. A. Maslov, S. G. Mironov, et al., "Hypersonic flow on a flat plate. Experimental results and numerical modeling," *Prikl. Mekh. Tekh. Fiz.*, **36**, No. 6, 60–67 (1995).
22. H. S. Tsien, "Aerodynamics of rarefied gases," in: *Gas Dynamics* [Russian translation], Izd. Inostr. Lit., Moscow (1950).